Quadrupolar nuclear magnetic resonance spectroscopy in solids using frequency-swept echoing pulses

Rangeet Bhattacharyya and Lucio Frydman[a)]
Department of Chemical Physics, Weizmann Institute of Science, 76100 Rehovot, Israel

(Received 16 July 2007; accepted 10 September 2007; published online 16 November 2007)

The acquisition of ideal powder line shapes remains a recurring challenge in solid-state wideline nuclear magnetic resonance (NMR). Certain species, particularly quadrupolar spins in sites associated with large electric field gradients, are difficult to excite uniformly and with good efficiencies. This paper discusses some of the opportunities that arise upon departing from standard spin-echo excitation approaches and switching to echo sequences that use low-power, frequency-swept radio frequency (rf) pulses instead. The reduced powers demanded by such swept rf fields allow one to excite spins in different crystallites efficiently and with orientation-independent pulse angles, while the large bandwidths of interest that are needed by the measurement can be covered, thanks to the use of broadband frequency sweeps. The fact that the spins' evolution and ensuing dephasing starts at the beginning of such rf manipulation calls for the use of spin-echo sequences; a number of alternatives capable of providing the desired line shapes both in the frequency and in the time domains are introduced and experimentally demonstrated. Sensitivity- and lineshape-wise these experiments are competitive vis-à-vis current implementations of wideline quadrupolar NMR based on hard rf pulses; additional opportunities that may derive from these ideas are also briefly discussed. © *2007 American Institute of Physics*.
[DOI: 10.1063/1.2793783]

I. INTRODUCTION

The anisotropic character of the spin interactions plays a central role in defining the line shapes observed in both nuclear magnetic resonance (NMR) and electron paramagnetic resonance measurements in solids.[1,2] Inhomogeneous broadenings such as those arising from the chemical shift, hyperfine, or quadrupolar anisotropies lead to characteristically broad line shapes; once suitably collected and analyzed, such powder patterns can provide valuable insight into the environments surrounding their originating sites. Collecting undistorted powder patterns, however, is not always a trivial proposition. Particularly challenging instances arise in the NMR of nuclides possessing quantum spin numbers $S>1/2$, which are often affected by large quadrupolar interactions C_Q.[1–5] These couplings depend on the asymmetry of the electric fields surrounding the nuclear sites and their effects may reach into the kilohertz or megahertz regime, thereby complicating the retrieval of undistorted line shapes. The severity of such effects can be attenuated when dealing with half-integer quadrupolar nuclei, whose central $-\frac{1}{2}\leftrightarrow+\frac{1}{2}$ transitions remain unaffected by first-order quadrupole effects $H_Q^{(1)}$. Still, even in these cases, central transitions are substantially broadened due to second order quadrupole effects, $H_Q^{(2)}$, as well as by anisotropic chemical shift terms H_{CS}. Overall, this leads to an orientation-dependent line shape which under ideal conditions is dictated by the central transition Hamiltonian[4,5]

$$H_{CT}=H_{CS}(\Omega)+H_Q^{(2)}(\Omega), \tag{1a}$$

with

$$H_{CS}(\Omega)=H_{iso}+C_{CSA}T_{20}^{CSA}R_{20}^{CSA}(\Omega^{CSA}) \tag{1b}$$

and

$$H_Q^{(2)}(\Omega)=-\frac{C_Q^2}{\gamma B_o}\sum_{m=-2}^{2}\frac{[T_{2m}^Q,T_{2-m}^Q]}{m}R_{2m}^Q(\Omega^Q)R_{2-m}^Q(\Omega^Q), \tag{1c}$$

containing the dependence of the resonance frequencies on the Euler angle sets Ω^λ subtended by each coupling tensor and the external field B_o. These, in turn, are summarized by the $\{R_{2m}\}_{-2\leqslant m\leqslant 2}$ spatial tensor elements, as well as by the $\{T_{2m}\}_{-2\leqslant m\leqslant 2}$ spin-space operators.

While an undistorted line shape arising from the H_{CT} Hamiltonian yields valuable information about the isotropic offset σ_{iso}, the shift anisotropy parameters δ_{CSA} and η_{CSA}, and the C_Q and η_Q values defining the quadrupole coupling, arriving at such spectral shape may be complicated due to nutation effects endowing different crystallites in the sample with different excitation angles—even if addressed by a common radio frequency (rf) pulse.[6,7] The origins of such nutation distortions are well understood,[6–9] and can be traced to the non-negligible first-order quadrupole effects that arise in the full rf-driven excitation Hamiltonian,

$$H_{exc}=H_{rf}+H_{CS}^{(\Omega)}+H_Q^{(1)}(\Omega)+H_Q^{(2)}(\Omega), \tag{2}$$

with $H_{rf}=-\nu_1 S_x$ representing the coupling to a rf field of intensity $\nu_1=\gamma B_1/2\pi$, and $H_Q^{(1)}=C_Q T_{20}^Q R_{20}^Q(\Omega)$. The fact that

a)Author to whom correspondence should be addressed. Tel.: +972-8-9344903. Fax: +972-8-9344123. Electronic mail: lucio.frydman@weizmann.ac.il

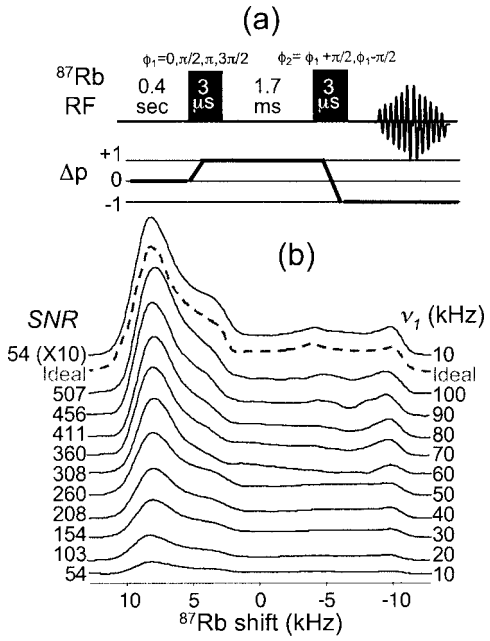

FIG. 1. (a) Two-pulse spin-echo pulse sequence exemplifying the effects of nutation distortions on the central transition line shapes of $S=3/2$ half-integer quadrupole nuclei. The indicated parameters were used, and the desired coherence transfer pathway was selected by the eight-scan phase cycle summarized. (b) Ideal (dashed trace) and experimental ^{87}Rb NMR line shapes collected on a static Rb_2SO_4 powder sample, as a function of the ν_1 rf irradiation field. The ideal line shape reflects two overlapping sites possessing quadrupolar coupling parameters $C_Q=2.72$ MHz, $\eta_Q=0.93$ and $C_Q=4.90$ MHz, $\eta_Q=0.15$, conforming to the single-crystal parameters of this salt (Ref. 10). Experimental traces were collected by signal averaging 512 transients (0.4 s recycle delay); notice that only those experiments recorded in the weak rf limit (e.g., at $\nu_1=10$ kHz) resemble the ideal line shape, even if these experiments exhibit the lowest SNRs.

these two main terms do not commute with one another leads to an excitation behavior depending on the $\nu_1/C_Q R_{20}^Q$ ratio; when taking into account the dependence of the R_{20}^Q second-rank Legendre polynomial on orientation, a complex excitation process results—not only for the satellite but also for the central transitions. As a consequence, the nutation angle θ imparted by the rf will, in general, depend on the relative orientation Ω between the magnetic field B_o and each crystallite, even if a single chemical site is considered. In fact, only in the extreme $\nu_1/C_Q \gg 1$ and $\nu_1/C_Q \ll 1$ cases will the excitation of the spins be uniform for all powder orientations. Otherwise, as illustrated by the experimental line shapes shown in Fig. 1 for the relatively "benign" ^{87}Rb NMR case of Rb_2SO_4, orientation- (i.e., frequency-)dependent distortions will affect the line shapes.

When taking these effects into account it follows that acquiring distortion-free quadrupolar powder line shapes would be facilitated by working in the $\nu_1/C_Q \gg 1$ (strong rf) regime. Yet unless one is dealing with unusually small quadrupole couplings, such strong irradiation conditions have seldom been fulfilled.[11] In a majority of instances, it has consequently been shown that using weak—and often, very weak—rf fields becomes a method of choice for obtaining undistorted quadrupolar powder patterns.[12] In such cases, the nutation rate imparted by the rf on the central transitions becomes $\nu_{nut}=(S+1/2)\nu_1$, regardless of crystallite orientation. As illustrated in Fig. 1 for the case of Rb_2SO_4, only when rf fields become weaker than ~10 kHz (corresponding to $\nu_1/(C_Q/[2S(2S-1)]) \approx 0.05-0.1$ ratios) will a conventional spin-echo sequence yield undistorted central transition powder line shapes. The use of such weak rf fields, however, poses problems of its own in terms of optimizing the rf pulse lengths. Given the weak rf fields needed by such protocol sensitivity would recommend using relatively long pulses; however, this in turn would lead to relatively narrow excitation bandwidths that would themselves become a source of "hole burning" and thereby of additional line shape distortions. On the other hand, short rf pulses, capable of homogeneously exciting the required wide frequency ranges, do not offer an optimal choice either: in combination with the weak fields required, they would entail small excitation/refocusing angles, associated with penalties in the resulting signal-to-noise ratio (SNR). A usual way out of this dichotomy employs a compromise between these two extremes, yielding neither a full excitation of the desired bandwidths nor the ideal $\theta=\pi/2$, π angles that one would wish to employ in optimized spin-echo sequences. The former complication can then be solved by arraying experiments over a series of properly chosen frequency offsets spreading over the targeted powder line shape,[13–15] while the latter is circumvented by the use of extended signal averaging. Both of these procedures will, naturally, increase the overall duration of the data acquisition process.

In an effort to better harmonize the conflicting low-power/large-bandwidth/optimal-excitation requirements demanded by this kind of experiment, this paper explores the possibilities that arise upon shifting the rf manipulations from fixed-frequency square pulses to frequency-swept pulses. Chirped pulses are used in a number of NMR scenarios toward the excitation and the decoupling of broad frequency ranges, a goal for which they are known to be especially well suited, as their nature is no longer bound by the *times x bandwidth*≈1 constraints of usual rf pulses.[16] In fact, excitation-oriented applications of chirped pulses were demonstrated early in the history of pulsed NMR,[17] with a number of elegant applications derived from even earlier field-swept NMR approaches.[1] Eventually, the broadband efficiency of frequency-swept RF manipulations found its most widespread usage in a number of liquid-state decoupling and refocusing NMR experiments,[18–24] as well as in *in vivo* imaging and spectroscopy.[25–28] Frequency-swept inversion pulses have also been explored in a number of solid-state NMR experiments, particularly toward the manipulation of central, satellite, and multiple-quantum coherences in quadrupolar nuclei.[29–32] Of relevance to the present study are the half-passage adiabatic sweep experiments of Kentgens and co-workers,[29,30] which evidenced several desirable SNR and line shape characteristics based on the use of a single-sweep (nonechoed) excitation. Further interest in frequency-swept manipulations has recently emerged with the realization of the important roles that these pulses, in combination with field gradients, could play toward the acquisition of two-dimensional NMR images and spectra within a single scan.[33–36] Using the notation developed during this latter set of investigations, the next sections explore two different experimental options that exploit these concepts for retrieving

undistorted powder patterns from the central transitions of half-integer quadrupoles.

II. EXPERIMENTAL

This work's data were acquired at 14.1 T (600 MHz ^{1}H frequency) on an InfinityPlus Varian® NMR spectrometer equipped with a 4 mm probe. The spectrometer could deliver shaped rf irradiation waveforms (up to 1024 points) over a range of Larmor frequencies, including those of ^{87}Rb and ^{35}Cl. The frequency sweeps required for this study were generated by the computer controlling the NMR instrument, which calculated within the pulse programs all necessary rf shapes as amplitude- and phase-modulated waveforms. These tables contained up to 900 phase and amplitude values equally spread over the duration of each pulse. Even for the largest bandwidths that were swept in our experiments (up to 200 kHz), the required waveform sampling times exceeded the minimum dwell times of the spectrometer's rf shaping tool (100 ns); further pulse sequence details are given and justified in the following paragraphs. Once experiments were completed data were exported from the instrument and processed off-line on a personal computer using custom-written MATLAB® and FORTRAN programs. Pulse sequences and processing scripts are available upon request.

III. RESULTS

A. Quadrupolar patterns by Fourier-transform of distortion-free powder echoes

We begin by considering the application of a rf excitation pulse whose offset O is linearly swept between initial and final values $O_i \rightarrow O_f$, over a time interval τ_{exc}. In order to make the effects of this rf sweep meaningful, we shall assume that the range it covers equals or exceeds the frequency spread of the pattern to be characterized; we shall also assume that this range is considerably larger than the pulse's duration-derived bandwidth τ_{exc}^{-1}; for instance, by taking $|O_f - O_i|\tau_{\mathrm{exc}} \geqslant 10-20$. Then, as the offset of such pulse reaches the orientation-dependent resonance frequency $f(\Omega)$ of a spin within the powder, this isochromat will become excited and begin its free precession.[16,37] As justified in further detail elsewhere, the overall phase ϕ_{exc} collected by the spins under such circumstances can be accurately described by the sum of two terms.[35,36] One involves the phase accrued by the rf up to the time $\tau(f)$ when its offset has reached a value of f; the other describes the spin's ensuing precession under the assumption of an instantaneous excitation and a subsequent free evolution. Assuming that the rf offset is swept at a constant rate R_{exc}, i.e., $O(t)=O_i+[(O_f - O_i)/\tau_{\mathrm{exc}}]t=O_i+R_{\mathrm{exc}}t$, the overall phase collected by spins resonating at a frequency f at the conclusion of the rf excitation will thus be

$$\begin{aligned}\phi_{\mathrm{exc}}(f) &= \phi_{\mathrm{rf}}[\tau(f)] + [\tau_{\mathrm{exc}} - \tau(f)]f \\ &= \int_0^{\tau(f)} [O_i + R_{\mathrm{exc}}t']dt' + \left[\tau_{\mathrm{exc}} - \left(\frac{f - O_i}{R_{\mathrm{exc}}}\right)\right]f \\ &= \left(\frac{O_i}{R_{\mathrm{exc}}} + \tau_{\mathrm{exc}}\right)f - \frac{f^2}{2R_{\mathrm{exc}}}, \end{aligned} \tag{3}$$

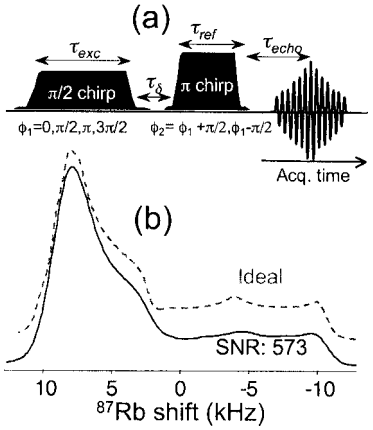

FIG. 2. (a) Frequency-swept full-echo pulse sequence proposed for the retrieval of undistorted central transition line shapes. The implemented coherence transfer pathway is similar to that in Fig. 1 and also achieved by suitable phase cycling. (b) Comparison between the ideally expected powder pattern and an experimental ^{87}Rb NMR spectrum acquired on Rb_2SO_4, using the indicated pulse sequence and the following parameters: τ_δ=0.1 ms, τ_{exc}=2.8 ms, and ν_1^{exc}=0.43 kHz for the $\pi/2$ pulse and ν_1^{ref}=2.02 kHz and τ_{ref}=1.4 ms for the π pulse, set according to sweep rates $|R_{\mathrm{exc}}|$ =12 kHz/ms and $|R_{\mathrm{ref}}|$=24 kHz/ms. Acquisition time was 3 ms (300 points with a 100 kHz spectral bandwidth) and 256 transients were recorded with a 0.4 s recycle delay. Out of these and in order to minimize potential distortions arising from transverse relaxation effects, 128 transients were collected with positive-valued R_{exc} and R_{ref} sweeps, and 128 were coadded with negative-valued sweep rates (following a reversal of their time axis).

where for simplicity, we have disregarded constant (i.e., f-independent) phase terms.

Equation (3) contains a quadratic frequency contribution, which will prevent the retrieval of a uniformed-phase signal from the full $|O_f - O_i|$ frequency bandwidth. Hence single-passage sweeps can suit the undistorted excitation of relatively narrow patterns[29,30] but will yield a substantial destructive interference among different spin packets (and hence little observable signal) when f's excursion is broad. To account for such dephasing we begin by exploring the refocusing proposal of Bodenhausen and co-workers that cancels out these effects by means of a subsequent π pulse,[18,19] also sweeping f between O_i and O_f but over its own refocusing interval τ_{ref}. Given the transverse state where this refocusing rf pulse finds the spins' magnetizations, its action on the spins' evolution will differ from that happening upon excitation, and will now be described by[34]

$$\begin{aligned}\phi_{\mathrm{ref}}(f) &= -\tau(f)f + 2\phi_{\mathrm{rf}}[\tau(f)] + [\tau_{\mathrm{ref}} - \tau(f)]f \\ &= \frac{(O_i + O_f)}{R_{\mathrm{ref}}}f - \frac{f^2}{R_{\mathrm{ref}}}, \end{aligned} \tag{4}$$

where the various parameters and calculations involved have meanings akin to those used in the excitation case. The overall frequency-dependent encoding resulting upon merging these two frequency-swept manipulations into a single pulse sequence [with the added provision for a small interpulse delay τ_δ Fig. 2(a)] is

$$\phi_{\mathrm{encoding}}(f) = \phi_{\mathrm{ref}}(f) - \phi_{\mathrm{exc}}(f) - \tau_\delta f, \tag{5}$$

where the minus signs reflect the inverting effects of the refocusing pulse. Following these rf-driven frequency-swept manipulations comes the acquisition time t, a period of free

evolution where spin coherences gain an additional tf term. The total phase defining the NMR signal will thus be

$$\Phi_{\mathrm{tot}}(f,t) = \phi_{\mathrm{encoding}}(f) + tf. \tag{6}$$

Assuming for simplicity symmetric chirps fulfilling rotating frame offsets $O_i = -O_f$, this total acquisition phase can be further simplified to

$$\Phi_{\mathrm{tot}}(f,t) = f^2\left(\frac{1}{2R_{\mathrm{exc}}} - \frac{1}{R_{\mathrm{ref}}}\right) - f\left(\frac{O_f}{R_{\mathrm{exc}}} + \tau_\delta\right) + ft. \tag{7}$$

It follows that the quadratic term preventing the formation of a simultaneous echo for all frequencies f in the powder can be canceled out by making the refocusing chirp rate twice as fast as its excitation counterpart: $R_{\mathrm{ref}} = 2R_{\mathrm{exc}}$. A f-independent echo then results for all crystallites at an acquisition time

$$\tau_{\mathrm{echo}} = \tau_\delta + \frac{O_f}{R_{\mathrm{exc}}} = \tau_\delta + \frac{\tau_{\mathrm{exc}}}{2}. \tag{8}$$

Within the context of quadrupolar NMR, it is worth exploring what role could the Fourier transform (FT) of the resulting echoes plays toward the acquisition of undistorted central transition line shapes. In other words, we explore whether the frequency-swept excitation/refocusing procedures just described can yield line shapes endowed with better SNRs than their conventional spin-echo counterparts, while operating under conditions that fulfill the weak rf regime required to obtain f-independent nutation angles. As detailed elsewhere,[26,27,35,37] the amplitudes required by a chirped rf to impart either a $\theta = \pi/2$ (nonadiabatic) or a $\theta = \pi$ (adiabatic) rotation of the spins depend on the square root of the sweeping rate R; for instance, for a spin-1/2 nucleus, the nutation field required for a $\pi/2$ excitation is $\nu_1 \approx 0.25\sqrt{R_{\mathrm{exc}}}$, while an in-plane π-type refocusing requires $\nu_1 \geqslant 0.8\sqrt{R_{\mathrm{ref}}}$. Since these chirped pulses are also characterized by large times x bandwidth products (as mentioned, usually in excess of 10), this, in turn, means that effective $\pi/2$ excitations will be feasible using rf pulses whose amplitudes ν_1 are between one and two orders of magnitude smaller than the $|O_i - O_f|$ bandwidths. Given such small ν_1 values, the weak rf field conditions desired for a uniform quadrupolar excitation end up fulfilled for most cases of practical interest. In fact, the only precaution that we found necessary upon extending the sequence in Fig. 2(a) from spin-1/2 species to the central transitions of half-integer quadrupoles involved a further downscaling of the rf amplitude so as to account for the nutation effects arising in the resulting weak-irradiation regime. This, in turn, is in accordance with what follows from a related quantum-mechanical analysis on the employment of adiabatic pulses, toward the manipulation of half-integer quadrupoles.[30] Rf fields were thus adjusted to $\nu_1^{\mathrm{exc}} \approx 0.25\sqrt{R_{\mathrm{exc}}/(S+1/2)}$ for executing $\theta = \pi/2$ excitation sweeps and to $\nu_1^{\mathrm{ref}} \approx 0.8\sqrt{R_{\mathrm{ref}}/(S+1/2)}$ for the subsequent π-driven refocusing. Figure 2(b) illustrates representative experimental results obtained upon taking such considerations into account, using once again the Rb_2SO_4 model compound as target of these measurements. As can be appreciated all nutation distortions have virtually disappeared from the resulting line shapes, owing to the very weak ν_1 fields required for imparting the $\pi/2$ and π rotation pulses. The SNR per unit time meanwhile has increased by a factor of ~10 vis-à-vis the weak rf square-pulse example in Fig. 1, thanks to the efficiency with which chirped procedures achieve a full excitation and refocusing of the spins.

B. Quadrupolar patterns from undistorted time-domain echo shapes

The option illustrated in Fig. 2(a) constitutes but one of the possibilities opened up by chirped rf manipulations toward the acquisition of wideline NMR spectra. Interesting features also arise upon departing from the $R_{\mathrm{ref}} = 2R_{\mathrm{exc}}$ condition. As follows from Eq. (7), Φ_{tot} will in such cases preserve a component that is quadratic in f, meaning that spin echoes will not form simultaneously for all crystallites in the powder but rather progressively; in an f-dependent, time-incremented fashion. In such cases, the signal collected from the sample at any given acquisition time t will only reflect those crystallites whose overall evolution phases do not vary rapidly throughout the powder spectrum. The frequency of these crystallites can be identified as that which, at any given time t, satisfies the stationary phase condition,

$$\frac{d}{df}[\Phi_{\mathrm{tot}}(f)]_{f=f_t} = 0. \tag{9}$$

Notice that the condition derived in Eq. (8) represents but a special case of this approximation, for the $d^2\Phi_{\mathrm{tot}}/df^2 = 0$ situation arising when $R_{\mathrm{ref}} = 2R_{\mathrm{exc}}$. Otherwise, when this is not the case, echoes will form progressively for separate frequencies within the powder sample as a function of the acquisition time t, according to

$$f_t = \frac{\tau_\delta + \frac{\tau_{\mathrm{exc}}}{2} - t}{\left(\frac{d^2\Phi_{\mathrm{tot}}}{df^2}\right)}. \tag{10}$$

This expression is a spectroscopic analog of the expression that we derived using spatial encoding arguments, within the context of single-scan multidimensional image acquisitions based on chirped rf pulses.[35,36] Following derivations analogous to those made in that imaging case, the time-domain signal collected in the solid-state NMR experiments here considered will be given by

$$S(t) \propto e^{i\Phi_{\mathrm{tot}}(f_t)} \sqrt{\frac{2\pi}{\left|\frac{d^2\Phi_{\mathrm{tot}}}{df^2}\right|_{f=f_t}}} I(f_t). \tag{11}$$

Given the linear relation between f_t and t [Eq. (10)], it follows that the NMR spectrum $I(f)$ becomes proportional to digitized $S(t)$ in a point-by-point fashion. The former can thus be retrieved from the latter simply by taking the magnitude of the resulting time-domain signal $|S(t)|$—no FT of the data being required.

As mentioned, the spectrum retrieval procedure embodied by Eq. (11) is analogous to the one that has been described in detail for the collection of spatially encoded images. Therefore, we shall only summarize here its main

characteristics, referring to Refs. 35 and 36 for more detailed discussions. Particular features that are worth noting include: (i) the exponential term in Eq. (11), which is not relevant for retrieving $I(f)$ spectra from $S(t)$ signals since the data processing involves a magnitude calculation $|S(t)|$. Moreover, since $\Phi_{\text{tot}}(f_t)$ is an *a priori* known quadratic phase-modulating function, its effects can be compensated entirely either by shifting the carrier frequency during the course of the acquisition or by a suitable postprocessing of the data. (ii) The second term in the right-hand side of Eq. (11) embodies an encoding-dependent constant, describing the minimum Δf separation that the method can distinguish. Its value, therefore, represents the protocol's frequency resolution, which ends up inversely dependent on the curvature of the parabolic phase profile subtended by Φ_{tot} throughout the powder. (iii) By giving up on the need for a FT the method rescinds the multiplex advantage,[38] thereby paying a price in terms of SNR. Still, this disadvantage can be largely counterbalanced by the fact that the spectral range needed to characterize the signal's intensity is no longer given by the full bandwidth of the powder pattern but rather by the Δf defined by the encoding parameters. Such feature can be exploited in practice, as further detailed below.

In an effort to shed further light on these features and on the potential of this new approach, a series of experiments was carried out under the $R_{\text{exc}}=R_{\text{ref}}$ condition. In such a case, the sweep rates of both the excitation and refocusing pulses can be maximized and made equal to a value R. Equation (10) then predicts that each crystallite will refocus at its own f-dependent echo time,

$$t_f = \tau_\delta + \frac{\tau_{\text{exc}}}{2} + \frac{f}{R}. \tag{12}$$

Notice that in this case, the frequency resolution (under the oversampling conditions that should usually be used in this kind of approach) and the maximum frequency bandwidth of the spectral characterization will be defined by $\Delta f=\sqrt{2\pi R}$ and by $|O_f-O_i|$, respectively, rather than by the usual acquisition-based Nyquist criteria. This encoding-defined dependence of the spectral characteristic parameters is not surprising when considering that the method shares many basic elements with stepped-frequency acquisitions,[13–15] where the maximum achievable bandwidths and frequency resolution considerations also end up depending on how the rf excitation has been set up, rather than on how data were physically digitized. Moreover, for a given $|O_f-O_i|$ bandwidth of interest, the spectral resolution Δf of the swept rf experiments becomes inversely proportional to the square root of the encoding time. This is again in contrast to what is observed in conventional FT NMR, where resolution ends up being inversely proportional to the actual evolution times. Figure 3 illustrates experimental results obtained with this approach, using once again the Rb_2SO_4 as model sample. Emphasis is paid here to the various stages involved in the processing of the data, as well as on the effects that changing the rate R (and thereby the maximum encoding time) will have on the spectral resolution. Notice that for the two experiments shown a $\tau_\delta=0.1$ ms delay was introduced for the sake of shifting the data, which were then digitized over a $0 \leqslant t \leqslant \tau_{\text{exc}}+\tau_\delta$ period. Shown on the leftmost panels are the as-collected experimental one-dimensional $S(t)$'s, characterized by a signal subtending nonzero values over an interval τ_{exc} and showing a fast quadratic phase modulation centered around $\tau_{\text{ex}}/2+\tau_\delta$ [for which $f=(O_i+O_f)/2$]. As only the amplitude of these signals is being sought this phase modulation can be removed by either an $e^{-i[\Phi_{\text{tot}}(t)]}$ phase correction or by a magnitude calculation (Fig. 3, center). Removing the fast phase modulations by either one of these procedures enables the aforementioned application of a simple frequency-domain filtration of the data with bandwidth Δf, which removes a substantial amount of noise from the $S(t)$ line shapes (Fig. 3, right). Absolute-value calculations then afford the powder patterns being sought, convoluted with a Gaussian point spread function whose width depends on $\tau_{\text{exc}}^{-1/2}$.

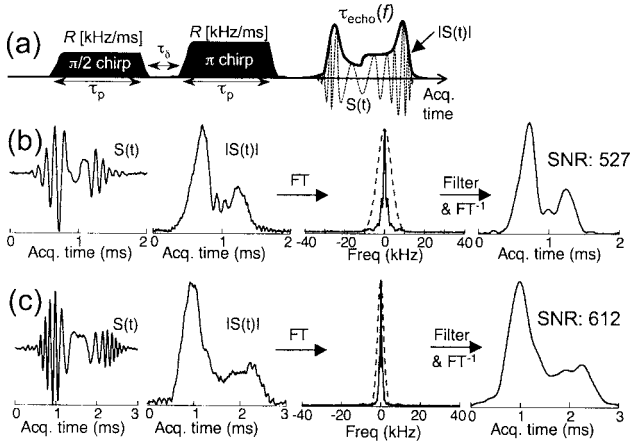

FIG. 3. (a) Frequency-swept-pulse sequence proposed for the retrieval of frequency-progressive echoes, yielding time-domain line shapes that reproduce the ideal frequency-domain powder patterns. The coherence transfer pathway, phase cycling, and recycling delay used were the same as in Fig. 2, and a positive- and negative-sweep coaddition strategy was once again used. (b) ^{87}Rb NMR data acquired from Rb_2SO_4 using the pulse sequence (a) with the following parameters: $\tau_\delta=0.1$ ms, $\tau_{\text{exc}}=\tau_{\text{ref}}=1.4$ ms, and $\nu_1^{\text{exc}}=0.6$ kHz for the $\pi/2$ pulse and $\nu_1^{\text{ref}}=2.0$ kHz for the π pulse set according to a common sweep rate $|R|=24.0$ kHz/ms. The leftmost panel is the as-recorded time-domain signal (real part, 256 scans, and 0.4 s recycle delays, 128 scans with positively valued R's and 128 scans with negatively valued R's), showing a strong quadratic modulation as a function of time. Next to it is a magnitude plot reflecting the sample's $I(f)$ powder line shape; this pattern's SNR can be further improved by FT, filtering to remove uninformative high-frequency components (for instance, by multiplication with what the dashed filtering function shows) and inverse FT (right). (c) Idem as in (b) but for a pulse sequence involving $\tau_{\text{exc}}=\tau_{\text{ref}}=2.8$ ms; i.e., $|R|=12.0$ kHz/ms, and $\nu_1^{\text{exc}}=0.43$ kHz and $\nu_1^{\text{ref}}=1.43$ kHz. Notice the increased spectral resolution Δf associated with this decrease in sweep rates.

IV. DISCUSSION

As mentioned, one of the driving forces that leads us to explore the data acquisition possibilities arising upon switching central transition solid-state NMR experiments from a square-pulse to a chirped-pulse format was the promise of obtaining line shapes that, while not distorted by the nutation frequency distributions characterizing the excitation pulses, possess an improved SNR. The experimental results in Figs. 1–3 validate these expectations; further benefits should derive from these approaches as the strengths of the couplings—and with these, the anisotropic broadening

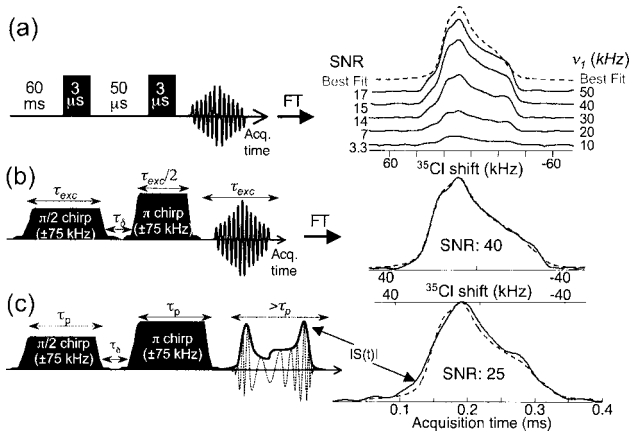

FIG. 4. Comparison between the different protocols discussed in this work, as pertaining to ^{35}Cl NMR spectroscopy on the single site arising in polycrystalline ornithine hydrochloride. (a) ^{35}Cl powder patterns obtained using a conventional square-pulse spin-echo approach with the indicated parameters, as a function of the rf field employed. (b) Full-echo pulse sequence and frequency-domain ^{35}Cl NMR line shape arising following FT, on using the following parameters: τ_δ=0.05 ms, τ_{exc}=0.3 ms, ν_1^{exc}=2.8 kHz, τ_{ref}=0.15 ms, ν_1^{ref}=13.0 kHz, and sweep rates $|R_{exc}|$=500 kHz/ms and $|R_{ref}|$=1000 kHz/ms. (c) Frequency-progressive echo pulse sequence and ensuing ^{35}Cl NMR time-domain line shape obtained with τ_δ=0.05 ms, τ_p=0.3 ms, ν_1^{exc}=2.8 kHz, ν_1^{ref}=9.2 kHz, and a common sweep rate R=500 kHz/ms. 500 000 transients separated by a 0.06 s recycle delay and 400 points digitized with 1 μs dwell time, were used in all experiments. The indicated SNRs were obtained in each case, following an optimized weighting of all data sets. Shown with dashed traces in all panels is the best fit arising from the experimental data, characterized by the following coupling parameters: C_Q=(4.1±0.1) MHz, η_Q=0.8±0.1, σ_{iso}=(185±2.5) ppm with respect to the Na^{35}Cl signal, δ_{CSA}=(175±5) ppm, η_{CSA}=1.0±0.1, and relative Euler angles orienting quadrupolar Ω^Q and shielding Ω^{CSA} tensor orientations of ψ=100±20, θ=150±10, and φ=180±20.

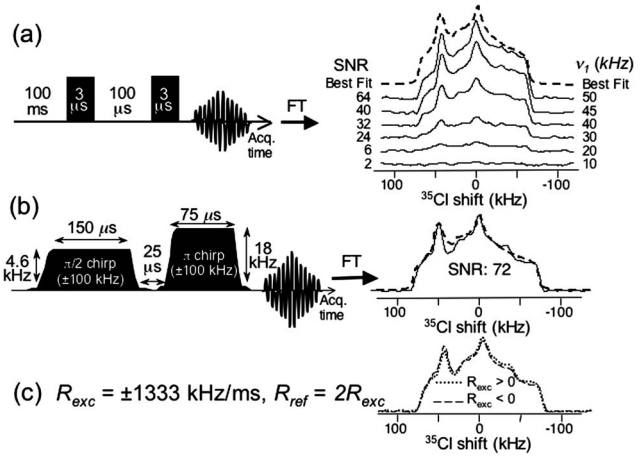

FIG. 5. Further comparisons between the hard-pulse and the frequency-swept-pulse spin-echo protocols, this time applied to ^{35}Cl NMR spectroscopy on polycrystalline glycine hydrochloride. (a) ^{35}Cl powder patterns obtained using a conventional square-pulse spin-echo approach as a function of the rf field. (b) ^{35}Cl NMR line shape arising by FT upon using the full-echo frequency-swept sequence with the indicated parameters (including ν_1 rf field strengths). This line shape arose by coadding two sets of data identical in all respects except for the sign of their rf sweep rates R_{exc} (and ensuing R_{ref}), which were +1333 kHz/ms for the dashed-line case and −1333 kHz/ms for the dotted line one shown in panel (c). Notice that although transverse spin relaxation effects bias the signal intensities of the resulting line shapes in opposite ways, such effects are compensated by their final coaddition. 20 000 transients separated by a 0.1 s recycle delay were used in all experiments [in case (c), 10 000 transients for each sweep direction], leading to the indicated SNRs following an optimized weighting of the data sets. Shown with dashed traces in panels (a) and (b) is the best fit arising from the experimental data, characterized by the following coupling parameters: C_Q=(6.5±0.1) MHz, η_Q=0.6±0.1, σ_{iso}=(101±4) ppm, δ_{CSA}=(86±5) ppm, η_{CSA}=0.2±0.1, and relative Euler angles orienting quadrupolar Ω^Q and shielding Ω^{CSA} tensor orientations of ψ=133±10, θ=90±10, and φ=100±10. These parameters are comparable to those recently reported for this salt in Ref. 39.

effects—increase. Figure 4 illustrates this point with a second set of examples based on ^{35}Cl NMR central transition acquisitions on L-ornithine hydrochloride, a salt whose sole chlorine site gives an ~70 kHz wide static pattern at 14.1 T fields. As illustrated by the various comparisons in the figure, applying the methods that we have hereby introduced alleviates nutation distortions, while simultaneously increasing the spectral SNR achievable per unit acquisition time. We believe that these advantages may help transform frequency-swept strategies of this sort, which to some extent represent continuous variants of more traditional multiscan frequency-stepped approaches, into methods of choice for the acquisition of certain kinds of wideline spectra.

At the same time, it is worth pointing out a number of potential drawbacks that may be associated with the "parallelism" embodied by the use of frequency-chirped pulses. These will mostly stem from the fact that, given the sequential manner by which crystallites in the sample are addressed in these experiments, their final spectral profiles will exhibit a higher sensitivity to transverse T_2 effects than in conventional spin-echo experiments. Indeed, in acquisitions such as those exemplified in Fig. 1, all crystallites are affected by a uniform interpulse delay τ and by a minor contribution arising from the pulse durations themselves. These durations can be decreased down to hardware-dictated values, meaning that the overall transverse evolution periods can be made very short. By contrast, in the sequences introduced in Figs. 2–4, each frequency f ends up associated with transverse evolution times governed by the durations chosen for the chirped rf pulses. Moreover, unlike in the classical scenario, the minimal lengths of such pulses will be constrained by the times x bandwidth product considerations deemed necessary for a proper operation of the rf chirps, rather than by hardware considerations. This, in turn, may bring about a number of complications, for instance, f-dependent powder pattern distortions associated with differential decays over opposite ends of the powder line shape. In the present study, such distortions were compensated by averaging signals arising from experiments that alternatively reversed the values of the O_i and O_f offsets (i.e., the sign of the R sweeps). Not taking such precaution may lead to minor line shape distortions, as illustrated in Fig. 5, with a series of ^{35}Cl NMR examples recorded on glycine hydrochloride. More difficult to remedy could be the overall signal losses associated with these swept-echo experiments. We have observed, for instance, that static experiments of the kind that were here described performed poorly *vis-à-vis* their standard hard-pulse counterparts when applied on certain fast-relaxing, narrow-bandwidth spin systems—particularly when involving abundant sites that are weakly affected by the nuclear quadrupole interaction, such as those encountered in simple ^{27}Al or ^{23}Na salts. This, in turn, reflects the relatively long times that are then needed for the two rf sweeps, going sometimes up to a

few milliseconds in duration, and the ensuing relaxation losses that arise from homonuclear interactions. In such cases, it is likely that swept half-passage or conventional spin-echo approaches will give better SNRs than the methods hereby discussed. On the other hand, such weakly coupled systems would not normally be targeted by the frequency-stepped static approaches that motivated the present work.

Another issue worth discussing concerns the relative merits of the two different chirped rf strategies introduced in Sec. III. In principle, the quality of the experimental results presented suggests that the frequency-domain line shapes arising from FT of the full-powder echo equal or exceed the quality achievable upon analyzing the time-domain line shapes (e.g., Figs. 2–4). This, in combination with the more usual data processing that the former method involves, seems to make it the better choice among the two. Still, a variety of situations could be envisioned where characterizing powder patterns in the time domain provides advantages over the more classical FT approach. The most evident one stems from the method's greater flexibility: it does not require setting the rates of the chirped pulses in accordance with one another, while providing a R-dependent scaling of the powder line shapes. Yet another, more subtle advantage could arise upon considering the maximum range of frequencies accessible to either approach. Limiting this range will be a number of factors including the console's capacity to deliver broadband frequency-swept rf waveforms, the console's capacity to receive a range of frequencies matching those that were transmitted, as well as the probehead's potential to accommodate these wide irradiation and detection ranges. Under normal operating conditions it will be the probe's response that confines the transmission and detection of very wide frequency ranges, as regular resonant circuits possess Q factors circumscribing the observable line shapes to at most a few percents of the Larmor frequency. While such frequency response will then set the ultimate frequency ranges that can be accessed by the approaches that were here described, there are, in fact, alternatives capable of facilitating the constant-rate sweep protocol described in Sec. III B to cover even wider spectral ranges. One such instance would arise upon rotating the powder sample at a rate ν_r; different crystallites will then "sweep" at different times through a constant-frequency rf pulse at rates on the order of $(C_Q^2/\gamma B_o)\nu_r$, leading to effects that are analogous to those arising upon sweeping the rf through a static powder pattern.[5,9,30,31,40,41] Such rotating-sample instance would then be freed from the probe's bandwidth constraints, and two constant-R sweeps could then be combined to yield an echo version of the experiment introduced in Sec. III B—but accessing a much wider range of frequency values than would be possible by sweeping rfs on a conventional probe. Similar echoing alternatives could also be considered involving a constant frequency but variable-field operation on a static sample, an option which could find applicability toward the characterization of very wide magnetic resonance line shapes originating from either nuclei or electrons. For all these manipulations, a time-domain characterization, compared to its variable-sweep FT-based counterpart, could result more suitabe to retrieve distortion-free powder patterns.

V. CONCLUSIONS

We have considered some of the new avenues that frequency-swept manipulations could open toward the characterization of broad NMR powder patterns. Such manipulations offer convenient approaches to carry out spin excitations and inversions when having to deal with sizable inhomogeneous broadenings in solids. It was shown, in particular, that opportunities arise when dealing with the acquisition of central transition quadrupolar line shapes, upon relying on experiments that use two chirped rf pulses instead of the more conventional fixed-frequency shapes. This operation can alleviate the conflicting demands placed by the presence of sizable couplings on the rf bandwidths, rf pulse strengths, and rf pulse durations. Different frequency-swept manipulations which could find applications in a number of realistic half-integer quadrupole NMR scenarios were demonstrated, and their potential limitations were discussed. Intriguing possibilities also arise upon considering counterpart experiments, where irradiation frequencies are fixed but resonance offsets are continuously changed by virtue of either sample spinning or field sweeps. Investigations into these and related research avenues are currently in progress.

ACKNOWLEDGMENTS

We are grateful to Mr. Yoav Shrot and Mr. Assaf Tal for insightful discussions regarding this project. This work was supported by the Israel Science Foundation (ISF 1206/05) and the German-Israel Fund for Research (GIF 782/2003), and made possible by the generosity of the Perlman family. R.B. acknowledges the Feinberg Graduate School (WIS) for a postdoctoral fellowship.

[1] A. Abragam, *The Principles of Nuclear Magnetism* (Oxford University Press, Oxford, 1961).
[2] C. P. Slichter, *Principles of Nuclear Magnetic Resonance*, 3rd ed. (Springer-Verlag, New York, 1990).
[3] M. H. Cohen and F. Reif, Solid State Phys. **5**, 321 (1957).
[4] A. Jerschow, Prog. Nucl. Magn. Reson. Spectrosc. **46**, 63 (2005).
[5] S. E. Ashbrook and M. J. Duer, Concept Magn. Res. **28A**, 183 (2006).
[6] A. Samoson and E. Lippmaa, Chem. Phys. Lett. **100**, 205 (1983).
[7] R. Janssen and W. S. Veeman, J. Chem. Soc., Faraday Trans. 1 **84**, 3747 (1988).
[8] A. P. M. Kentgens, J. Magn. Reson., Ser. A **104**, 302 (1993).
[9] A. J. Vega, in *Encyclopedia of NMR*, edited by D. M. Grant and R. K. Harris (Wiley, Chichester, 1996), p. 3869.
[10] T. Vosegaard, J. Skibsted, H. Bildsoe, and H. J. Jakobsen, J. Magn. Reson., Ser. A **122**, 111 (1996).
[11] K. Yamauchi, J. W. G. Janssen, and A. P. M. Kentgens, J. Magn. Reson. **167**, 87 (2004).
[12] P. P. Man, J. Klinowski, A. Trokiner, H. Zanni, and P. Papon, Chem. Phys. Lett. **151**, 143 (1988).
[13] T. J. Bastow, Solid State Nucl. Magn. Reson. **3**, 17 (1994).
[14] A. Medek, V. Frydman, and L. Frydman, J. Phys. Chem. A **103**, 4830 (1999).
[15] J. A. Tang, J. D. Masuda, T. J. Boyle, and R. W. Schurko, ChemPhysChem **7**, 117 (2006).
[16] M. Garwood and L. DelaBarre, J. Magn. Reson. **153**, 155 (2001).
[17] J. J. Dunant and J. Delayre, U.S. Patent No. 3,975,765 (August 1976).
[18] J.-M. Bohlen, M. Rey, and G. Bodenhausen, J. Magn. Reson. **84**, 191 (1989).
[19] L. Ermakov, J.-M. Bohlen, and G. Bodenhausen, J. Magn. Reson. **103**,

226 (1993).
[20] R. Fu and G. Bodenhausen, Chem. Phys. Lett. **245**, 415 (1995).
[21] R. Fu and G. Bodenhausen, J. Magn. Reson., Ser. A **117**, 324 (1995).
[22] E. Kupce and R. Freeman, J. Magn. Reson., Ser. A **115**, 273 (1995).
[23] E. Kupce and R. Freeman, J. Magn. Reson., Ser. A **117**, 246 (1995).
[24] E. Kupce and R. Freeman, J. Magn. Reson., Ser. A **118**, 299 (1996).
[25] C. J. Hardy, W. A. Edelstein, and D. Vatis, J. Magn. Reson. **66**, 470 (1986).
[26] D. Kunz, Magn. Reson. Med. **3**, 377 (1986).
[27] R. A. de Graaf, Y. Luo, M. Terpstra, H. Merkle, and M. Garwood, J. Magn. Reson., Ser. B **106**, 245 (1995).
[28] J. G. Pipe, Magn. Reson. Med. **33**, 24 (1995).
[29] A. P. M. Kentgens, J. Magn. Reson., Ser. A **95**, 619 (1991).
[30] E. VanVeenendaal, B. H. Meier, and A. P. M. Kentgens, Mol. Phys. **93**, 195 (1998).
[31] G. Wu, D. Rovnyak, and R. G. Griffin, J. Am. Chem. Soc. **118**, 9326 (1996).
[32] D. Iuga, H. Schäfer, R. Verhagen, and A. P. M. Kentgens, J. Magn. Reson. **147**, 192 (2000).
[33] L. Frydman, T. Scherf, and A. Lupulescu, Proc. Natl. Acad. Sci. U.S.A. **99**, 15858 (2002).
[34] A. Tal, B. Shapira, and L. Frydman, J. Magn. Reson. **176**, 107 (2005).
[35] Y. Shrot and L. Frydman, J. Magn. Reson. **172**, 179 (2005).
[36] A. Tal and L. Frydman, J. Magn. Reson. **181**, 179 (2006).
[37] C. Barratt, E. D. Fackerell, and D. Rosenfeld, J. Magn. Reson. **85**, 35 (1989).
[38] A. G. Marshall and F. R. Verdun, *Fourier Transforms in NMR, Optical, and Mass Spectrometry: A User's Handbook* (Elsevier, Amsterdam, 1990).
[39] D. Bryce, G. D. Sward, and S. Adiga, J. Am. Chem. Soc. **128**, 2121 (2006).
[40] T. Gullion and A. J. Vega, Prog. Nucl. Magn. Reson. Spectrosc. **47**, 123 (2005).
[41] C. P. Grey, W. S. Veeman, and A. J. Vega, J. Chem. Phys. **98**, 7711 (1993).